Certain Metal Ions Are Inhibitors of Cytochrome b_6f Complex 'Rieske' Iron−Sulfur Protein Domain Movements†

Arthur G. Roberts,‡ Michael K. Bowman,‡,§ and David M. Kramer*,‡

Institute of Biological Chemistry, Washington State University, 289 Clark Hall, Pullman, Washington 99164-6340, and WR Wiley Environmental Molecular Sciences Laboratory, Pacific Northwest National Laboratory, Richland, Washington 99352-0999

Received November 29, 2001; Revised Manuscript Received January 31, 2002

ABSTRACT: Many current models of the Q cycle for the cytochrome (cyt) b_6f and the cyt bc_1 complexes incorporate 'Rieske' iron−sulfur protein (ISP) domain movements to gate electron transfer and to ensure high yields of proton shuttling. It was previously proposed that copper ions, which bind at a site distant from the quinol oxidase (Q_o) site, inhibit plastoquinol (PQH_2) binding by restraining the hydrophilic head domain of the ISP [Rao B. K., S., Tyryshkin, A. M., Roberts, A. G., Bowman, M. K., and Kramer, D. M. (1999) *Biochemistry 38*, 3285−3296]. The present work presents evidence that this is indeed the case for both copper ions and Zn^{2+}, which appear to inhibit by similar mechanisms. Electron paramagnetic resonance (EPR) spectra show that Cu^{2+} and Zn^{2+} binding to the cyt b_6f complex displaces the Q_o site inhibitor 2,5-dibromo-3-methyl-6-isopropylbenzoquinone (DBMIB). At high concentrations, both DBMIB and Cu^{2+} or Zn^{2+} can bind simultaneously, altering the Rieske 2Fe2S cluster and Cu^{2+} EPR spectra, suggesting perturbations in their respective binding sites. Both Zn^{2+} and Cu^{1+} altered the orientations of the Rieske 2Fe2S cluster with respect to the membrane plane, but had no effect on that of the cyt b_6 hemes. Cu^{2+} was found to change the orientation of the cyt *f* heme plane, consistent with binding on the cyt *f* protein. Within conservative constraints, the data suggest that the ISP is shifted into a position intermediate between the ISP_C position, when the Q_o site is unoccupied, and the ISP_B position, when the Q_o site is occupied by inhibitors such as DBMIB or stigmatellin. These results support the role of ISP domain movements in Q_o site catalysis.

The cytochrome (cyt)[1] b_6f complex, which is analogous both in structure and in function to the mitochondrial and bacterial cyt bc_1 and *bc*-type complexes, plays a central role in photosynthetic electron transport in cyanobacteria and plant chloroplasts (for reviews, see *1*−*9*). It serves three main functions: (1) It transfers electrons from plastohydroquinone, or plastoquinol (PQH_2), to a soluble carrier, plastocyanin (PC) or a *c*-type cyt, which delivers them to photosystem (PS) I. (2) It uses the free energy available in the electron-transfer reactions to shuttle protons from the stroma (*n*-side) to the lumen (*p*-side), contributing to the establishment of proton motive force (*pmf*), which drives the synthesis of ATP. (3) It acts as a redox sensor, initiating antenna state transitions when the plastoquinone (PQ) pool becomes predominantly reduced (*10*−*13*).

The cyt b_6f complex is comprised of four major protein subunits: the cyt *f* protein, the 'Rieske' iron−sulfur protein (ISP), the cyt b_6 protein, and subunit IV (*14*). In the cyt bc_1 complex, the latter two are fused into a single analogous protein, known as the cyt *b* subunit. Both the cyt b_6 and the cyt *b* subunits house one low-potential cyt *b* heme (cyt b_L) and one high-potential cyt *b* heme (cyt b_H). The cyt *f* subunit contains an unusual *c*-type heme with one axial ligand supplied by the protein N-terminal amino group (*15*) and is functionally analogous to the cyt c_1 protein in the mitochondrial cyt bc_1 complex. The ISP houses a 'Rieske'-type iron−sulfur cluster (2Fe2S), which is coordinated by two histidines and two cysteines. Several smaller subunits, chlorophyll, and carotenoid molecules have also been found in the cyt b_6f complex, but their functions are not well understood (*1*, *16*−*18*).

The cyt b_6f complex also contains two PQ/PQH_2 binding sites which function during normal turnover to oxidize PQH_2 at the quinol oxidase (Q_o) site and reduce PQ at the quinol reductase (Q_i) site. The Q_i site is formed by the cyt b_6 protein, and subunit IV, toward the *n*-side of the membrane (i.e., stroma) (reviewed in *1*, *3*, *4*, *14*). The analogous site in the cyt bc_1 complexes is found in the cyt *b* subunit. The Q_o site of the cyt b_6f complex is at the interface between cyt b_6 and the Rieske ISP and adjacent to the *p*-side of the membrane

† This work was supported by U.S. Department of Energy Grant DE-FG03-98ER20299, by a Frasch Foundation award (D.M.K.), and by NIGMS Grant GM61904 (M.K.B.). The WR Wiley Environmental Molecular Sciences Laboratory is a national scientific user facility sponsored by the Department of Energy's Office of Biological and Environmental Research and located at Pacific Northwest National Laboratory.

* Corresponding author. Phone: ++(509) 335-4964; Fax: ++(509) 335-7643; Email: dkramer@wsu.edu.

‡ Washington State University.

§ Pacific Northwest National Laboratory.

[1] Abbreviations: cyt, cytochrome; cyt b_L, low-potential *b* cytochrome; cyt b_H, high-potential *b* cytochrome; DBMIB, 2,5-dibromo-3-methyl-6-isopropylbenzoquinone; DMSO, dimethyl sulfoxide; DNP-INT, 2-iodo-6-isopropyl-3-methyl-2′,4,4′-trinitrodiphenyl ether; EPR, electron paramagnetic resonance; HEPES, *N*-(2-hydroxyethyl)piperazine-*N*′-2-ethanesulfonic acid; ISP, iron−sulfur protein; *pmf*, proton motive force; PC, plastocyanin; PQ, plastoquinone; PQH_2, plastoquinol; PS, photosystem; Q_i, quinol reductase; Q_o, quinol oxidase; UHDBT, 5-*n*-undecyl-6-hydroxy-4,7-dioxobenzothiazole.

10.1021/bi015996k CCC: $22.00
Published on Web 03/03/2002

(i.e., thylakoid lumen). Several inhibitors bind strongly to this site, including stigmatellin, 5-*n*-undecyl-6-hydroxy-4,7-dioxobenzothiazole (UHDBT), 2-iodo-6-isopropyl-3-methyl-2′,4,4′-trinitrodiphenyl ether (DNP-INT), and 2,5-dibromo-3-methyl-6-isopropylbenzoquinone (DBMIB) (*2*−*4, 19*).

Electron transfer through the complex occurs through a process known as the Q-cycle, first proposed by Mitchell (*20*), and later modified by several groups (see reviews *21*−*26*). Electron transfer from the Q_o site quinol is bifurcated, so that one electron is transferred to the 'high potential chain', consisting of the 2Fe2S cluster and cyt *f*, while the other is forced through the 'low potential chain' consisting of cyt b_L and cyt b_H to a quinone at the Q_i site. This results in the release of two protons from the Q_o site quinol into the chloroplast lumen, contributing to *pmf* that drives ATP synthesis.

The yield of the bifurcated electron transfer and proton pumping in the higher plant cyt b_6f complex is high both in vitro (*27*) and in vivo (*28*), implying that reactions which bypass the Q-cycle are minimized. Since transferring both quinol electrons to the high-potential chain would be heavily favored by thermodynamics (see discussions in *27, 29*), it has long been proposed that a 'catalytic switch' gates electron transfer at the Q_o site, to force electron flow down the two pathways (*30, 31*). The recent structural and functional advances in our understanding of the cyt bc_1 complex offer an intriguing explanation for such a catalytic switch. Different crystal forms and crystals made in the absence and presence of Q_o site inhibitors showed that the hydrophilic 'head' domain of the ISP occupies several different positions. One position, termed ISP_B, places the ISP close to the distal niche of the Q_o site; another, termed ISP_C, places the ISP close to cyt c_1; still others place the ISP in intermediate positions (*2, 32*−*35*). Molecular dynamics simulations of the ISP in these structures showed that the ISP likely rotates freely around a central 'pivot' by 57°−63° (*36*). This pivoting action of the ISP is thought to prevent the transfer of both electrons from the quinol to the high-potential chain, and is consistent with the observed electron-transfer rates (*33, 36*). Electron transfer between quinol bound at the Q_o site and the nearby 2Fe2S cluster, while in the ISP_B configuration, should produce a reduced 2Fe2S cluster and a semiquinone at the Q_o site, locking it into this configuration (as suggested in *33, 37*−*40*). As long as the ISP is prevented from adopting the ISP_C position, reoxidation of the 2Fe2S cluster would be hindered by the large cluster to cyt c_1 heme distance, leaving cyt b_L as the only available oxidant for the semiquinone. Conversely, when in the ISP_C position, the 2Fe2S cluster is too far from the Q_o site to allow oxidation of the QH_2 or the semiquinone. Thus, coordinated motion of the ISP head domain between the ISP_B and ISP_C positions is key to the operation of the Q-cycle. We note that, although the cyt b_6f complexes contain cyt *f* instead of cyt c_1, we retained the term ISP_C to be consistent with the cyt bc_1 literature.

It has been known for many years that Zn^{2+} and other divalent metal ions inhibit cyt bc_1 complexes (*41*−*45*). In previous work, we showed that Cu^{2+} inhibits the cyt b_6f complex (*46*). There are important differences between the mechanisms of metal inhibition of the cyt bc_1 and cyt b_6f complexes. Link et al. (*41*) found that Zn^{2+} inhibition of the cyt bc_1 complex was noncompetitive with either quinol or cyt *c* substrates. This, together with the pH-dependence of the K_i, suggested that Zn^{2+} may act by blocking proton release from the Q_o site. Since then, Berry et al. (*47*) showed that avian mitochondrial cyt bc_1 complex contains at least two Zn^{2+} binding sites: one near the Q_o site, which was hypothesized to cause inhibition, and the other close to the interface between cyt *b* and cyt c_1.

In contrast, our work has shown that inhibition of the spinach cyt b_6f complex by Cu^{2+} (*46*) and Zn^{2+} (see below) was competitive with the substrate PQH_2, but noncompetitive with PC or horse heart cyt *c*, suggesting substantially different mechanisms for inhibition. One great advantage of Cu^{2+} as an inhibitor is that it is paramagnetic, allowing us to use pulsed-EPR techniques to probe its binding site. With these techniques, we showed that Cu^{2+} binds to a histidine residue (*46*). A structural model of the cyt b_6f complex (cf. Figure 10 of *46*), based on homology modeling to the X-ray crystal structures of the mitochondrial cyt bc_1 complex (*33*) as well as the structures of the cyt b_6f complex ISP (*48, 49*) and cyt *f* protein (*3, 15*), suggested that the Cu^{2+} binding site was probably on cyt *f* or the ISP. Because these residues lie distant from the Q_o site, we concluded that Cu^{2+} binding displaces PQH_2, probably via longer-range conformational changes that are transmitted through the ISP (*46*). Thus, we proposed that metal ions inhibit the turnover of the cyt b_6f complex by restraining normal ISP domain movements.

MATERIALS AND METHODS

Thylakoid Preparation. Spinach thylakoids were prepared essentially as described in (*27*) with one modification. In the final stage, the thylakoid pellet was resuspended in HCL buffer [i.e., 30 mM *N*-(2-hydroxyethyl)piperazine-*N*′-2-ethanesulfonic acid (HEPES, pH 7.6), 0.5% cholic acid, 0.1% α-lecithin] with 10% $(NH_4)_2SO_4$ and 5−10% dimethyl sulfoxide (DMSO) to a concentration of greater than 4 mg mL^{-1} chlorophyll and stored at −80 °C. The chlorophyll content of the thylakoids was determined by the method of Arnon (*50*). The choice of HEPES buffer was critical since many other buffers chelate Cu^{2+} and other metals, preventing strong interaction with the cyt b_6f complex (*51*).

Purification of the Cyt b_6f Complex. Cytochrome b_6f complex was isolated from spinach thylakoids essentially as described by Hurt and Hauska (*52, 53*) with some modifications. Thylakoids at 3 mg mL^{-1} chlorophyll were solubilized with HCL buffer containing 40−60 mM *n*-octyl glucoside and 10% $(NH_4)_2SO_4$ and incubated 30 min on ice in the dark. The precise concentration of detergent was determined for each thylakoid batch as the concentration required for the release of ∼90% cyt b_6f complex from the membranes (*53, 54*). Detergent-solubilized suspensions were centrifuged at 141000*g* for 30 min at 4 °C. Then this was diluted with HCL buffer containing 40% $(NH_4)_2SO_4$ to the supernatant to give a final concentration of $(NH_4)_2SO_4$ of 25%. Ammonium sulfate fractionation was performed with most of the cyt b_6f precipitating in the 45−55% fraction as has been previously described (*53*). The pellet was resuspended in HCL buffer with 30 mM *n*-octyl glucoside. This was dialyzed for 1 h against HCL buffer containing 10 mM *n*-octyl glucoside to remove the $(NH_4)_2SO_4$. The detergent *n*-octyl glucoside was added slowly to the dialyzed samples to a final concentration of 30 mM, and the resulting suspension was placed onto a sucrose density gradient, 7−30%, which was prepared by freeze−thaw technique using HCL buffer with 30 mM

n-octyl glucoside and was centrifuged at 141000*g* for 12−16 h at 4 °C. After centrifugation, the resulting brown band in the sucrose density gradient was assayed for activity and cyt *f* concentration as previously described in (*46*). The brown band was then dialyzed against HCL buffer with 10 mM *n*-octyl glucoside for 1 h to remove the sucrose. Then the *n*-octyl glucoside was added to the dialyzed protein until the final concentration was 30 mM. The suspension was then concentrated to 10−30 μM cyt *f*, using a 100 kDa cutoff Amicon Centricon concentrator (Millipore, Inc., Bedford, MA), and then stored with 20% glycerol at −80 °C. The activity of the complex was measured as described in (*46*) with turnover of ∼30 s^{-1} at 100 μM cyt *c*.

Preparation of Oriented Cyt b_6f Complex. Partially ordered samples were obtained from purified cyt b_6f complex as reported previously (*37*, *55*−*58*). A stock suspension of ∼30 μM cyt b_6f complex was dissolved in 25 mL of 30 mM HEPES, to a final concentration of approximately 0.4 μM cyt b_6f complex. This was centrifuged for 14 h at 141000*g* and 4 °C. The pellet was then dissolved in 25 mL of distilled, deionized water and centrifuged for 30 min at 141000*g* and 4 °C. Inhibitors, including 10 μM Cu^{2+} or Zn^{2+}, were added at this step. The resulting pellet was resuspended with a small amount (∼50−200 μL) of deionized, distilled water. This was applied to strips of Mylar (type A, Dupont Co., Wilmington, DE) with a small paintbrush and allowed to dry for 3 days under argon above 80% w/v $ZnCl_2$ to maintain humidity.

To reduce the 2Fe2S cluster or Cu^{2+}, while maintaining the cyt *b* hemes oxidized, the strips were dipped momentarily in a 10 mM solution of sodium ascorbate buffered with 30 mM HEPES (pH 7.6). To obtain oxidized samples, where the cyt *b* and cyt *f* were oxidized, strips were briefly dipped in 5 mM sodium ferricyanide buffered with 30 mM HEPES (pH 7.6). After dipping, strips were allowed to dry under Ar(g) for several minutes. Several strips were then stacked and placed in an EPR tube and quickly stored at −80 °C.

EPR Spectroscopy. Electron paramagnetic spectra were obtained using a Bruker 200tt EPR spectrometer (Bruker Instruments, Billerica, MA), using a GFS-300 transfer tube, ESR-900 helium cryostat with model ITC4 temperature controller (Oxford Instruments, Oxford, U.K.). The data were acquired using a CIO-DAS1401/12 digital I/O board (Computer Boards, Inc. Mansfield, MA) connected to a Pentium PC computer and software written in Microsoft Visual Basic 6.0 (Microsoft, Redmond, WA). The EPR acquisition parameters are provided in the figure legends. The orientation of the Mylar sheets within the magnetic field was adjusted and measured using a Varian E-229 goniometer (Varian, Inc., Palo Alto, CA) with an accuracy of about ±1°.

EPR Spectral Simulations of Oriented Samples. The EPR spectra of the oriented membrane samples were simulated in a two-step procedure, using Mathematica Version 4.1 (Wolfram Research, Champaign, IL) and standard equations (*59*). First, the EPR frequency, Ω, of the ISP or other paramagnetic center was scaled with respect to its values, ω, at g_{max} and g_{min} as

$$Y(\Omega) = \frac{\Omega - \omega(g_{min})}{\omega(g_{max}) - \omega(g_{min})}$$

so that in the absence of inhomogeneous broadening of the EPR spectrum, $0 \le Y \le 1$. A second scaled parameter, $f = Y(g_{mid})$, characterizes the rhombicity, or deviation from axial symmetry of the *g*-tensor. When the magnetic field makes angles of θ and ϕ with respect to the g_{max} and g_{min} axes of the ISP, the EPR frequency, *Y*, is $Y(z,\phi) = f^*(1 - z^2)^*\sin(\phi)^2 + z^2$ where $z = \cos(\theta)$. Assuming isotropic inhomogeneous broadening of the EPR transition described by a Gaussian function with width proportional to dν, the natural logarithm of the un-normalized EPR intensity at the scaled frequency, ν, of an ISP at an arbitrary orientation is $\ln EPR(z,\phi,\nu) = -[Y(z,\phi) - \nu/d\nu]^2$. The logarithm of the intensity is a much more smoothly varying function than the EPR intensity itself and provided much faster convergence in constructing an interpolating function for lnEPR within the cube defined over $0 \le z \le 1$, $0 \le \phi \le \pi/2$, and $0 \le \nu \le 1$ using Mathematica. This interpolating function then allows rapid integration over *z* and ϕ for calculation of the EPR spectrum of an arbitrary range of orientations.

If the ISP adopts a favored orientation, then the 2Fe2S *g*-tensor axes with respect to the membrane will be defined by a set of Euler angles, $(0,\xi,\psi)$. The preferred axis will deviate from the membrane perpendicular by an angle θ' due to disorder or mosaic spread with a relative probability $\exp[-(\theta'/m)^2]$ where *m* parametrizes the mosaic spread. In the spectrometer, the magnetic field is at an angle α with respect to the membrane perpendicular. Thus, the magnetic field is related to the 2Fe2S cluster *g*-tensor, and thus the ISP, by the Euler angles $(0,\alpha,\beta)$. The angle β takes on all possible values because the ISP molecules are aligned only with respect to one direction. The probability of finding an ISP oriented at (z,ϕ) with respect to the magnetic field in a membrane oriented with an angle α between its perpendicular and the magnetic field is given by

$$P(z,\phi,\alpha) = \int_0^{2\pi} \exp\left[-\left(\frac{\arccos(F[\beta])}{m}\right)^2\right] \cdot d\beta$$

where

$$F(\beta) = \cos(\alpha)\cdot[z\cdot\cos(\xi) + \sqrt{1 - z^2}\cdot\cos(\phi - \psi)\cdot\sin(\xi)] + \sin(\alpha)\cdot\{\cos(\beta)\cdot[\sqrt{1 - z^2}\cdot\cos(\phi - \psi)\cdot\cos(\xi) - z\cdot\sin(\xi)] + \sqrt{1 - z^2}\cdot\sin(\phi - \psi)\cdot\sin(\beta)\}$$

and the full symmetry with respect to *z* and ϕ was used to fold the unit sphere into a single quadrant. Another interpolating function in Mathematica was fit to $P(z,\phi,\alpha)$, and the intensity at any point in the EPR spectrum for a membrane at angle α is then readily calculated from the two interpolating functions as

$$I(\nu,\alpha) = \int\int P(z,\phi,\alpha)\cdot\exp[\ln EPR(z,\phi,\nu)]\, dz d\phi$$

For the polar plots, experimental data were compared with $I(1,\alpha)$ and $I(0,\alpha)$ at g_{max} and g_{min}, respectively, and to $2^*I(f,\alpha) - I(f+0.02, \alpha) - I(f-0.02,\alpha)$, which is proportional to the finite-difference approximation to the second derivative, at g_{mid}. Each simulated polar plot was normalized so that the maximum value was unity for comparison to data.

Use of a Gaussian function for the mosaic spread and an isotropic line width represent major limitations of these simulations. The mosaic spread in orientations has contributions from less than perfect orientation of the proteins within the membranes, including defects in the membrane such as

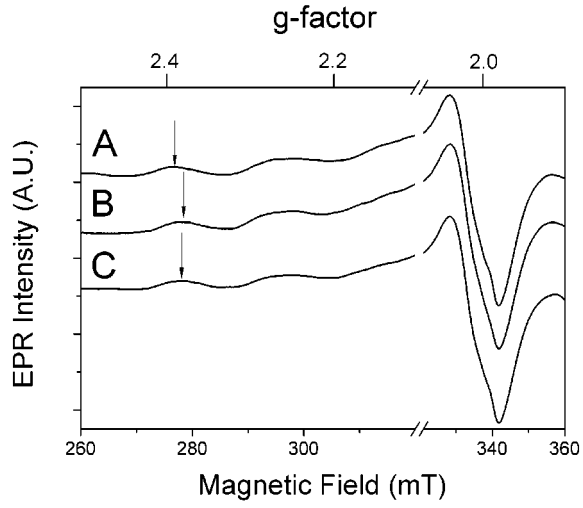

FIGURE 1: Effect of Q_o site inhibitors on cyt b_6f complex bound Cu^{2+} EPR signal. EPR spectra of Cu^{2+} bound to 30 μM cyt b_6f complex in (A) uninhibited, (B) 1 equiv (30 μM) of DBMIB, and (C) 1 equiv (30 μM) of stigmatellin. Arrows in the figure emphasize differences between the $g_{||}$ hyperfine peaks. EPR spectrometer settings were: microwave frequency = ~9.429 GHz; microwave power = 6.32 mW; gain = 4.0×10^5; time constant = 1000 ms; modulation amplitude = 1.6 mT; center field = 370 mT; sweep width = 200 mT; sweep time = 2 min; averages = 32; temperature = 70 K.

holes, folds, edges, and inclusions and also irregularities in the surface of the Mylar sheets. It is unlikely that the actual distribution is Gaussian; however, given the relatively large values of *m* needed to simulate the rotational plots, the actual distribution function is likely to be broad and featureless. The EPR spectrum of the ISP has a large amount of *g*-strain that is not included in the line width model. To do so would make the simulations much slower without improving the results given the level of approximations in the mosaic spread function. To fit the data, the simulations were superimposed on the experimental data at 1−5° angle increments with a mosaic spread between $0.250*\pi$ and $0.350*\pi$. The closest fits were determined by eye to have a mosaic spread of $0.275*\pi$ and angles that are described in the text.

RESULTS

Effects of Q_o Site Occupancy on Cu^{2+} Ligand Geometry. Figure 1 shows EPR spectra of Cu^{2+} bound to the cyt b_6f complex (unoriented samples) in the absence or presence of the Q_o site inhibitors DBMIB and stigmatellin. In the absence of inhibitors, the Cu^{2+} EPR spectrum was essentially as previously observed (*46*), and typical of type II Cu^{2+} spectra (for reviews, see *60*−*64*). The $g_{||}$ hyperfine line shapes indicate that two Cu^{2+} forms contribute to the observed spectra. The relative amounts of each form depend on the sample pH (Rao B. K., S., Tyryshkin, A. M., Kramer, D. M., and Bowman, M. K., unpublished data). These samples were prepared without ferricyanide to avoid overlap of its broad EPR signal at $g = \sim 2.7$ (*60*, *65*). The Cu^{2+} $g_\perp$ transition was found at $g = 2.04$ with a line width of 14 mT, both in the absence and in the presence of DBMIB or stigmatellin. In the absence of Q_o site inhibitors (Figure 1, trace A), the $g_{||}$ transition was found at $g = 2.22$ with average Cu^{2+} hyperfine splittings of $A_{||} = 2.21 \times 10^{-2}$ cm^{-1}. In the presence of DBMIB (Figure 1, trace B), $g_{||}$ was shifted to $g = \sim 2.225$ with $A_{||} = 2.04 \times 10^{-2}$ cm^{-1}. On the other hand, in the presence of stigmatellin (Figure 1, trace C), $g_{||}$ was shifted to $g = \sim 2.235$ with $A_{||} = 1.98 \times 10^{-2}$ cm^{-1}. Since the $g_{||}$ region is sensitive to the ligand environment of the Cu^{2+} (*60*, *63*, *66*−*68*), we concluded that introducing inhibitors into the Q_o site induced significant changes to the Cu^{2+} binding site.

In samples in Figure 1, the 2Fe2S EPR signal showed only a small g_y signal at $g = 1.89$, indicating that the cluster was predominantly oxidized. In any case, samples prepared with ferricyanide or with a slight excess of ascorbate to reduce the ISP but not Cu^{2+} showed nearly identical Cu^{2+} EPR spectra, albeit with different contributions in the Cu^{2+} $g_\perp$ region from the reduced 2Fe2S cluster (data not shown). From this, we concluded that the redox state of the 2Fe2S cluster did not have large effects on the ligand geometry of bound Cu^{2+}.

Zn^{2+} as an Inhibitor of the Cyt b_6f Complex. As demonstrated above, the EPR-sensitivity of Cu^{2+} makes it a sensitive probe of its structural environment. However, for other experiments, Cu^{2+} can be a less than an ideal inhibitor. The free (*69*) and cyt b_6f complex-bound (*46*) Cu^{2+}/Cu^{1+} couples are readily reduced by reductants such as ascorbate. Cu^{1+} reacts rapidly with O_2 to produce superoxide (see *70*, *71*), which can damage enzymes. In addition, the EPR spectrum of Cu^{2+} may overlap with other paramagnetic centers of interest. For these reasons, we also studied the effects of Zn^{2+}, which is not redox-active within physiological conditions and does not reduce O_2 (see *72*).

Kinetic assays showed that Zn^{2+} is competitive with PQH_2 and noncompetitive with cyt *c*, as we found earlier for Cu^{2+} but with K_I values somewhat higher than Cu^{2+} (~4 μM at 1 μM decyl PQH_2, A. G. Roberts and D. M. Kramer, in preparation). Although the inhibitory binding sites may differ, we propose that Zn^{2+} inhibits by the same general mechanism as copper. Because Zn^{2+} is diamagnetic, we were not able to use EPR to probe its binding site on the cyt b_6f complex.

Effects of Copper and Zinc on the Rieske 2Fe2S EPR Spectrum in the Absence of Q_o Site Occupants. In the absence of Q_o site inhibitors, addition of inhibitory concentrations of Cu^{1+}, Cu^{2+}, and Zn^{2+} had no apparent effects on the EPR spectrum of the reduced 2Fe2S cluster (data not shown). Such shifts would imply strong or direct interaction with the 2Fe2S cluster (see reviews *37*, *73*, *74*). These results are consistent with previous studies of copper, which found that the metal was bound far from the Q_o site and the 2Fe2S cluster (*46*).

Effects of Cu^{2+} and Zn^{2+} on the DBMIB-Induced Shifts of the Rieske 2Fe2S EPR Spectrum. Figure 2 shows EPR spectral changes of the 2Fe2S cluster upon addition of metals and the Q_o site inhibitor DBMIB. Addition of 2 equiv of DBMIB per complex was sufficient to induce the large, well-known changes in the EPR spectrum (Figure 2, trace A) with the appearance and increase of the $g = 1.94$ signal and the decrease in the $g = 1.89$ signal, as has been previously demonstrated (*39*, *75*, *76*). The concentration of ascorbate was kept low to prevent reduction of free DBMIB [E_m(pH 8.0) = ~60 mV, (*77*)] to its quinol form, which binds weakly to the complex (*39*). In the presence of DBMIB, the g_z transition around $g = 2.03$ showed distinct heterogeneity, expressed as an apparent second peak near $g = 1.99$, which was previously attributed to a free radical signal (*39*).

When Cu^{2+} and Zn^{2+} were added to DBMIB-treated complex, relatively large changes in the 2Fe2S spectrum were

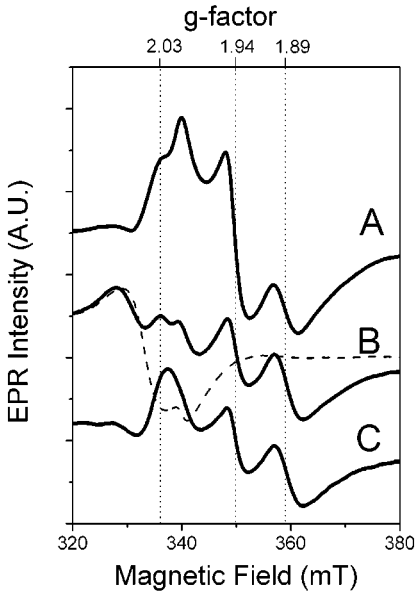

FIGURE 2: Effect of metals on the DBMIB-shifted "Rieske" 2Fe2S EPR spectrum. EPR spectra of the 2Fe2S cluster (25 μM cyt b_6f complex) with 2 equiv (50 μM) of DBMIB and (A) no metals, (B) 2 equiv (50 μM) of Cu^{2+}, or (C) 4 equiv (100 μM) of Zn^{2+}. Trace 2B (dotted line) shows the spectrum of Cu^{2+}-bound cyt b_6f complex spectra without reductants, where the 2Fe2S cluster was oxidized, illustrating the overlap of Cu^{2+} and 2Fe2S EPR spectra. EPR spectrometer settings were the same as in Figure 1 except the temperature was 20 K.

observed (Figure 2, traces B and C). Upon addition of equimolar concentrations of Cu^{2+} and DBMIB to the complex, the $g = 1.89$ transition showed an increase in line width to 5.5 mT from 4.0 mT and shifted upfield by 0.5 mT to $g = \sim 1.88$. The amplitude of the transition at $g = \sim 1.88$ increased with respect to the $g = 1.94$ transition in these samples, indicating that a fraction of the DBMIB was displaced (see *78*) or that the ISP was no longer interacting strongly with the DBMIB. Unfortunately, the significant signal overlap from the Cu^{2+} EPR spectrum (see Figure 2, trace B, dotted line) prevented a thorough analysis of changes in the 2Fe2S $g_z = 2.03$ transition or the $g = 1.94$ transition.

Addition of a 4-fold excess of Zn^{2+} caused similar shifts in the 2Fe2S spectrum of DBMIB-treated complex (Figure 2, trace C), but in this case without introducing interfering EPR signals. The amplitude of the transition at $g = \sim 1.88$ also increased with concomitant decrease in the $g = 1.94$ transition as was seen in the Cu^{2+}-inhibited samples. Furthermore, the $g = \sim 1.88$ transition line width increased to ~ 5.5 mT, similar to the Cu^{2+}-inhibited samples. This was accompanied by a decrease in the $g = 1.94$ signal that is characteristic of the displacement of DBMIB (*78*). Furthermore, the g_z transition at $g = 2.03$ appeared to shift to $g = 2.01$. Additions of higher concentrations of Cu^{2+} or Zn^{2+} led to nonspecific binding (*46*) and precipitation of the metal (data not shown, see also *79*) and were thus not useful for these studies.

Similar experiments were also performed with Cu^{1+}, but they were problematic because of the high concentrations of ascorbate that were used to keep the Cu^{1+} reduced also reduced DBMIB to its quinol form.

Orientation of the Redox Carriers of the Cyt b_6f Complex Estimated by EPR Spectroscopy of Mylar-Oriented Cyt b_6f Complex. Figure 3A shows 2Fe2S EPR spectra of oriented

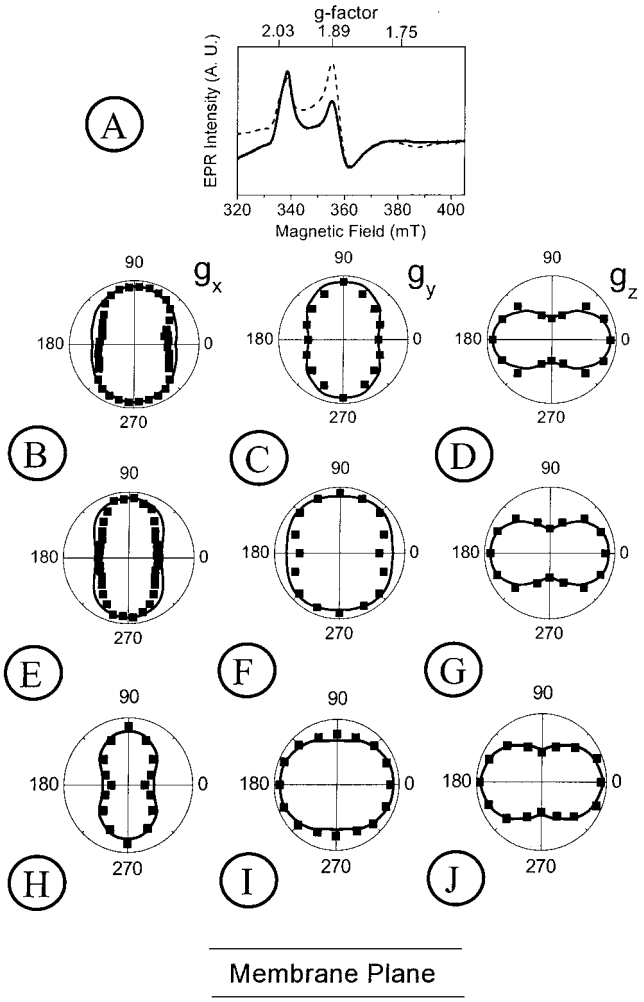

FIGURE 3: Orientations of the "Rieske" 2Fe2S cluster in the presence of metals. (A) EPR spectra of the "Rieske" 2Fe2S cluster in partially oriented samples of cyt b_6f complex in the absence of metals with magnetic field at 0° (solid line) and 90° (dashed line) with respect to the membrane plane. The g_x, g_y, and g_z transitions are found at 1.75, 1.89, and 2.03, respectively. Plots B−J show the angular dependence of the three EPR transitions on the angle of the magnetic field with respect to the membrane plane. The experimental data are shown as points, and the simulations (see Materials and Methods) are shown as solid lines superimposed on the experimental data. Data were taken in the absence of metals (plots B−D) and in the presence of Cu^{1+} (plots E−G) or Zn^{2+} (plots H−J). The orientation dependencies of g_x are shown in plots B, E, and H, those for g_y are shown in plots C, F, and I, and those for g_z are shown in plots D, G, and J. The orientation of the membrane plane with respect to the plots is shown at the bottom of the figure. For reliable determinations of the orientation dependence of the g_x transition, the amplitude of the transition was measured from a horizontal baseline drawn from 425 to 430 mT. EPR spectrometer settings were as in Figure 2, and a goniometer was used to orient the samples (see Materials and Methods).

cyt b_6f complex in the absence of inhibitors with the magnetic field oriented at 0° (solid line) and 90° (dotted line) with respect to the membrane plane. There was significant anisotropy of all three, $g_x = 1.75$, $g_y = 1.89$, and $g_z = 2.03$, transitions. In Figure 3B−D, the magnetic field-orientation dependence of these transitions is plotted with respect to the membrane plane. The *g*-axis orientations are similar to those reported earlier (*37, 39*).

Production of Mylar-oriented cyt b_6f complex with Cu^{2+} and reduced (paramagnetic) 2Fe2S was not reproducible because of the reduction of Cu^{2+} or the oxidation of the

2Fe2S cluster. Therefore, assays were performed with excess ascorbate, where Cu^{2+}, based on EPR analysis, was probably reduced to Cu^{1+} (*80*). The orientation dependence of the EPR transitions of samples containing at least some Cu^{2+} as determined by EPR analysis gave virtually identical results (data not shown). In addition, kinetic assays with Cu^{1+} suggested qualitatively that Cu^{1+} also acts competitively with PQH_2 and noncompetitively with the mobile redox carriers, PC and cyt *c*, although it is complicated because Cu^{1+} can subsequently reduce both of these mobile redox carriers (*80*).

Samples with Cu^{1+} or Zn^{2+} showed significant changes in the apparent orientations of the g_x, g_y, and g_z axes with respect to the membrane plane (Figure 3E−G and 3H−J). We attempted to simulate the orientation-dependence of the EPR spectra assuming a single orientation of the ISP 2Fe2S cluster. As described under Materials and Methods, we manually superimposed the simulated orientation dependence of the EPR transitions against the experimentally determined orientation dependence, until reasonable fits were obtained. Even the best fits showed small but significant deviations from the data. There are several possible explanations for these deviations, including non-Gaussian mosaic spread (see above) or multiple 2Fe2S cluster orientations. Nevertheless, these simulations qualitatively revealed the effects of metals on ISP conformation. The simulations suggested that for the metal-free control samples, the g_x, g_y, and g_z transition axes of the 2Fe2S cluster were at 41°, 43°, and 18°, respectively, away from the membrane plane, which is consistent with previous results (*37, 39*). Addition of metal ions shifted all three *g* axes, to approximately 45°, 37°, and 22° for Cu^{1+} and to 48°, 32°, and 24° for Zn^{2+}, respectively.

The ferricytochrome *f* EPR transition at $g_z = 3.5$, which lies perpendicular to the heme plane (*81*−*83*), was used to probe the orientation of the cyt *f* protein with respect to the membrane plane. Figure 4A shows the EPR spectra of the oriented sample in the $g = 3.5$ range with the magnetic field oriented at 0° and 60° with respect to the membrane plane, representing the minimal and maximal amplitudes, respectively (see below). Figure 4B is a plot of the orientation dependence of the g_z transition of cyt *f* with respect to the membrane plane. In control samples, the maximum amplitude of the cyt *f* g_z transition was found at 60°, implying that the heme plane lies at 30° from the membrane plane as previously reported in (*37, 81, 83*). Binding of Cu^{2+} clearly shifted the g_z transition by about 5° to ∼55°, indicating a shift in the orientation of the heme plane from 30° to ∼35° with respect to the membrane plane upon binding of Cu^{2+}. This is consistent with a Cu^{2+} binding site on the cyt *f* subunit as suggested in (*46, 80*).

The overlapping g_z transitions of both ferrocytochromes b_L and b_H are found at $g_z = 3.6$ (*81, 83*) and were used to probe the orientations of both cyt *b* hemes. Figure 5A shows EPR spectra in the $g = 3.6$ region with the magnetic field at 0° and 90° with respect to the membrane plane. Figure 5B shows the orientation of the $g_z = 3.6$ signal (*37*) with respect to the membrane plane. The maximum amplitude of the g_z signal was observed at ∼0°, implying that the planes of the cyt *b* hemes are oriented nearly perpendicular (*82*) to the membrane plane, as expected from previous EPR results (*37*) and models of the cyt b_6f complex (*3, 4, 84*). The orientations of the g_z transitions were virtually unchanged by Cu^{1+} with excess ascorbate, indicating that this metal did not perturb

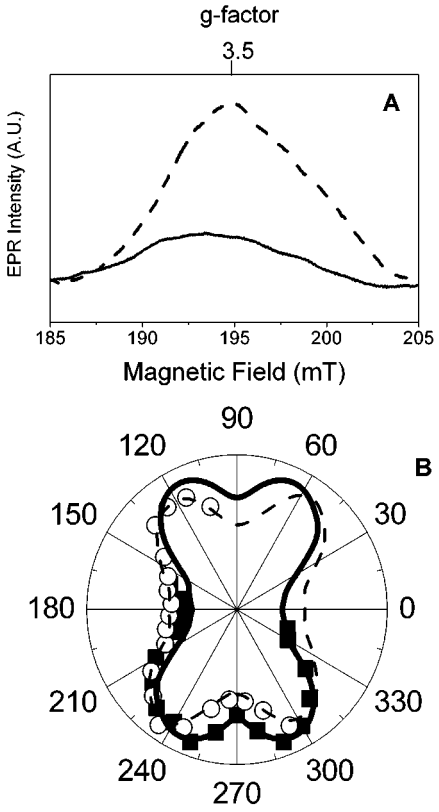

FIGURE 4: Effect of Cu^{2+} on the orientation of the cyt *f* g_z transition. (A) EPR spectra of the cyt *f* g_z transition in partially oriented samples of cyt b_6f complex in the absence of metals with magnetic fields at 0° (solid line) or 60° (dashed line) with respect to the membrane plane. (B) Rotational plot of the cyt *f* heme EPR $g_z = 3.5$ transition with respect to the membrane plane determined as for the 2Fe2S cluster (Figure 3) in the absence (solid line and closed squares) and presence of Cu^{2+} (dashed line and open circles). EPR spectrometer settings were the same as in Figure 2, except modulation amplitude = 3.2 mT; center field = 210 mT; sweep width = 200 mT; averages = 16; microwave power = 1 mW.

the membrane-spanning domains of the complex, including cyt b_6 and subunit IV. These experiments were repeated in the presence of excess ferricyanide, where both copper and cyt *f* are in their paramagnetic forms (i.e., Cu^{2+} and ferricytochrome *f*). In this case, careful analysis of the EPR spectra was required because of overlap with the cyt *f* g_z =3.5 signal. Nevertheless, no apparent effect was seen upon binding of Cu^{2+} on the orientations of the cyt *b* hemes (data not shown). Likewise, the addition of Zn^{2+} had virtually no effect on the orientation of the g_z transitions (data not shown). Under conditions used to bind these metals, it is clear that these metals do not significantly disrupt the orientation of the complexes on the Mylar sheets.

DISCUSSION

Much has been learned from the use of inhibitors which block specific partial reactions of the cyt *bc* and cyt b_6f complexes (reviewed in *1, 85, 86*). For example, specific inhibitors first allowed the elucidation of the essential functions of the two Q_o site niches and the Q_i site (*87*−*91*). In addition, such inhibitors have allowed the complex to be poised or trapped in important intermediate states of turnover for detailed spectroscopic study (e.g., *89, 92*).

Metal ions represent a distinct class of cyt *bc* and cyt b_6f complex inhibitors (*41*−*45*). Our work suggested that Cu^{2+}

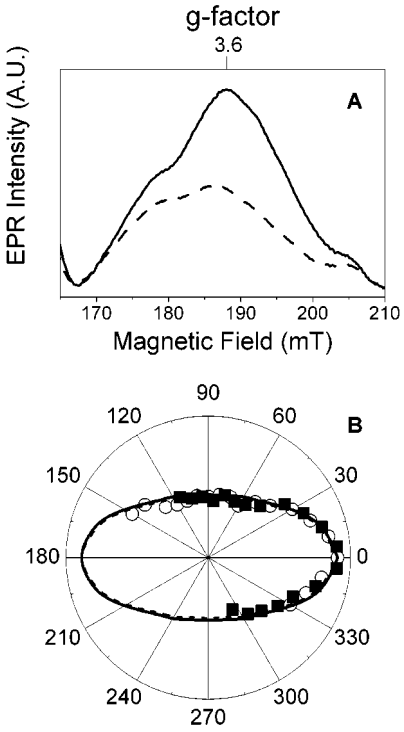

FIGURE 5: Effect of metals on the orientation of the cyt *b* heme g_z transition. (A) EPR transitions of the cyt *b*'s at $g_z = 3.6$ in the absence of metals with magnetic field at 0° (solid line) and 90° (dashed line) with respect to the membrane plane. (B) Orientational dependence of the $g_z = 3.6$ transition was determined as described in Figure 4, in the absence (solid line and closed squares) and presence of Cu^{1+} (dashed line and open circles). EPR spectrometer settings were the same as in Figure 4 except the microwave power was 20 mW.

and Zn^{2+} inhibit PQH_2 binding to the Q_o site of the cyt b_6f complex by long-range conformational changes (*46*). We proposed a model wherein ISP pivoting transmitted 'allosteric' effects of the metal from their distant binding sites to the Q_o site. In essence, we proposed that certain metal ions are specific inhibitors of ISP domain movements, restraining the ISP into distinct positions.

Metal Ions Affect the Conformation of the 2Fe2S Cluster of the 'Rieske" ISP. The data in Figure 3 confirm that metals shift the ISP into distinct positions. To better illustrate these conformational changes, we assigned the directions of the EPR transitions to the specific molecular axis of the 2Fe2S cluster. There is some disagreement in the literature concerning this issue (*74, 93*−*95*). Based on pulsed-EPR spectroscopy of the 'Rieske-type' 2Fe2S cluster in phthalate dioxygenase, Hoffman and co-workers (*93, 94*) suggested that the g_z transition lies along the Fe−Fe axis. On the other hand, Bertrand et al. (*95*), using ligand field analysis, suggested that the g_x transition occurs along the Fe−Fe axis. The latter assignment is more consistent with conclusions drawn from comparisons of the orientations of the 'Rieske' 2Fe2S cluster EPR transitions (*37, 39, 96*) with the orientation of the 'Rieske' 2Fe2S cluster in the X-ray crystal structures of the cyt bc_1 complex (e.g., *33*). More recent pulsed and oriented EPR results (M. K. Bowman, A. G. Roberts, and D. M. Kramer, in preparation) also suggest assignments in line with the X-ray structures (*39*), and we tentatively assign g_x, g_y, and g_z to the Fe−Fe, through the plane formed by the 2Fe2S and S−S directions, respectively.

Scheme 1: Proposed Hypothetical Effects of Metals and Q_o Site Inhibitors on the Orientation of the 2Fe2S Cluster and the Soluble Head Domain of the ISP[a]

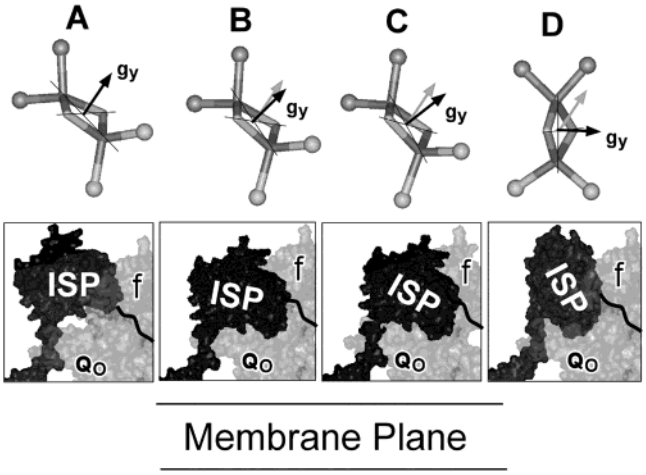

[a] Ball-and-stick models of the 2Fe2S cluster (top) and solvent-accessible surface (bottom) of the ISP (black) and the other subunits of the complex (gray) were generated based on X-ray structures of the cyt bc_1 complex (e.g., *33*), and oriented based on the data in Figure 3 and the molecular model described in (*46*). The cyt *f* protein and the Q_o site region are designated f and Q_o, respectively. The diagrams show the proposed 2Fe2S cluster orientations and the ISP head domain orientations with respect to the membrane plane, in the (A) absence of inhibitors or metals, (B) presence of copper, (C) presence of Zn^{2+}, and (D) presence of the Q_o site inhibitors, DBMIB or stigmatellin. The orientation of the membrane plane is shown with respect to the above diagrams. The arrows in the upper panels show the tentative orientation of the g_y EPR transition of the 2Fe2S cluster (see text for details). For comparison, the gray arrows indicate the orientation of the g_y axis in the control.

Scheme 1 illustrates the proposed effects of metals, copper and Zn^{2+}, and Q_o site inhibitors on the orientation of the 2Fe2S cluster and the hydrophilic head domain of the ISP. Using the above molecular axis assignments, the data in Figures 3 suggest that the addition of Cu^{1+} or Zn^{2+} pivoted the ISP roughly around the S−S axis, by about 7° (Scheme 1, B) and about 11° (Scheme 1, C), respectively. Oriented EPR studies of cyt b_6f complexes indicated that addition of stigmatellin or DBMIB induced rotation of the ISP around the same (S−S) axis by approximately 60° (as shown in Scheme 1, D), consistent with a shift from the ISP_C to ISP_B positions (*33, 37, 39*).

Since the complexes were inherently rotationally disordered within the plane of the membrane, it was not possible to determine from our EPR data whether the rotations induced by metal ions and Q_o site occupants were in the same direction. However, in the context of the cyt bc_1 X-ray structure and models of the cyt b_6f complex, the most conservative hypothetical position of the soluble head domain of the ISP would be one which would minimize unfavorable distortions of the neck region of the ISP and would be reasonably close to the Q_o site (*4, 33, 46, 97*). Therefore, we propose that the rotations of the ISP induced by inhibitory metals were in the same general direction as those induced by Q_o site occupants.

Projecting the approximate rotation data onto the various X-ray crystal structures of the cyt bc_1 complex suggests that inhibitory metals lock the ISP into intermediate positions, similar to those observed in some X-ray structures (*98*). Within the context of our model as described in (*46*), such

Scheme 2: Simplified Working Model of the Thermodynamic Relationship between Q_o Site Occupants and Metals[a]

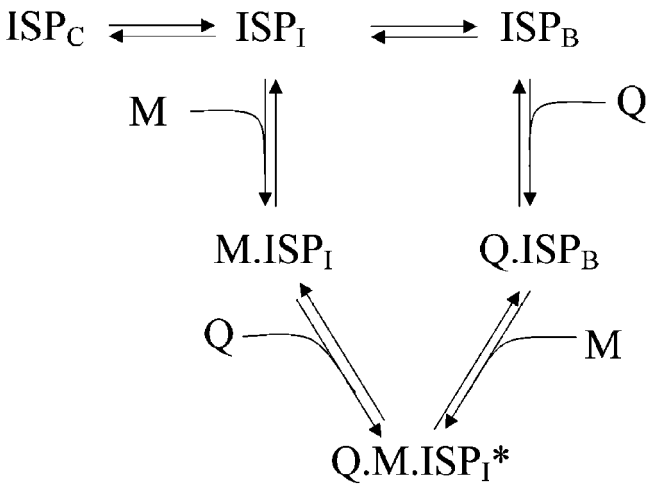

[a] The positions of the soluble head domain of the ISP are represented by ISP_C, ISP_I, ISP_I*, and ISP_B. A range of other ISP positions is possible (see text), but not shown for clarity. M and Q are metals and Q_o site occupants, respectively. The M·ISP_I, Q·ISP_B, and Q·M·ISP_I* states refer to the positions of the ISP, when metals, Q_o site occupants, and both are bound, respectively. A more detailed description of the thermodynamic relationships is given in the text.

constrained intermediate positions would likely reduce the affinity of quinol for the Q_o site and would strongly support the role of ISP domain movements in Q_o site catalysis.

Thermodynamics of Inhibitory Metals and Q_o Site Occupants. We propose a thermodynamic relationship between metals and Q_o site occupants as diagrammed in Scheme 2. In the absence of metals and distal Q_o site occupants, the hydrophilic head domain of the ISP can adopt a range of positions between two extremes, ISP_C and ISP_B (reviewed in *32*, *36*). We have designated two distinct intermediate positions between these two extremes, the ISP_I and ISP_I* positions, which can preferentially bind metal ions. When Q_o site occupants, such as quinol or DBMIB, are bound at the distal niche of the Q_o site, the ISP appears to be restrained by hydrogen bonding to the ISP_B position (*33*, *37*−*39*). This is designated the Q·ISP_B state in Scheme 2. In the absence of inhibitors under reducing conditions, the cyt bc_1 and cyt b_6f complex ISP tends to adopt the ISP_C position (*29*, *39*). We proposed that bound metals (M), Zn^{2+}, Cu^{2+} and Cu^{1+}, lock the head domain of the ISP into intermediate positions, which we have collectively designated the M·ISP_I state.

By shifting the ISP head domain into the M·ISP_I position, copper ions and Zn^{2+} would lower the binding affinity of quinol or Q_o site inhibitors at the Q_o site. Likewise, Q_o site occupants should interfere with metal binding by shifting the ISP into the Q·ISP_B state. This is consistent with the competitive behavior of Cu^{2+} (*46*) and Zn^{2+} (see above) observed in kinetic assays with the substrate PQH_2. It is also consistent with the apparent displacement of DBMIB from the Q_o site by Cu^{2+} and Zn^{2+} (Figure 2).

Because high concentrations of cyt b_6f complex were used in our EPR studies (25−30 μM), we suggest that at least some metals and Q_o site occupants are bound to the complexes simultaneously, but in perturbed conformations. Consistent with this, binding of stigmatellin (Figure 1, trace C) and DBMIB (Figure 1, trace B) induced significant distortions in the Cu^{2+} binding site as deduced by changes in the $g_{||}$ region of the cyt b_6f-bound Cu^{2+} EPR spectra. Both Zn^{2+} and Cu^{2+} induced complementary changes in the conformation of the bound Q_o site occupant, DBMIB, as shown by shifts in the *g*-transitions of the DBMIB-shifted 2Fe2S EPR spectrum (Figure 2). Assuming that these metal ions bind at exclusive sites far away from the Q_o site as shown for Cu^{2+} (*46*), we propose that simultaneous binding of both Q_o site occupants and metals shifts the ISP into a distinct position, which we have designated M·Q·ISP_I*.

We have previously concluded that Cu^{2+} binds to a histidine possibly on cyt *f* or the ISP, but far from the Q_o site itself (*46*). It is not clear precisely how Cu^{2+} binding to this residue could shift the ISP. We observed that copper ions shift the orientations of both the ISP and cyt *f* (Figures 3 and 4). There are two obvious explanations for this. First, the metal ion could directly interact with both subunits, though this appears incompatible with our hypothetical structural model of the cyt b_6f complex (*46*). Second, the metals could bind exclusively on one or the other protein. Since cyt *f* and the ISP are likely to interact, secondary mutual effects on the orientation may be expected.

ACKNOWLEDGMENT

We are indebted to Dr. R. Malkin for the donation of his 200tt EPR spectrometer to our laboratory. We thank Drs. W. Nitschke and M. Brugna for valuable discussions and technical assistance in this work.

REFERENCES

1. Hauska, G., Schutz, M., and Buttner, M. (1996) in *Oxygenic Photosynthesis: The Light Reactions* (Ort, D. R., and Yocum, C. F., Eds.) pp 377−398, Kluwer Academic Publishers, Dordrecht, The Netherlands.
2. Berry, E. A., Guergova-Kuras, M., Huang, L.-S., and Crofts, A. R. (2000) *Annu. Rev. Biochem. 69*, 1005−1075.
3. Cramer, W. A., Martinez, S. E., Huang, D., Tae, G.-S., Everly, R. M., Heymann, J. B., Cheng, R. H., Baker, T. S., and Smith, J. L. (1994) *J. Bioenerg. Biomembr. 26*, 31−47.
4. Soriano, G. M., Ponamarev, M. V., Carrell, C. J., Xia, D., Smith, J. L., and Cramer, W. A. (1999) *J. Bioenerg. Biomembr. 31*, 201−213.
5. Hope, A. B. (2000) *Biochim. Biophys. Acta 1456*, 5−26.
6. Trumpower, B. L., and Gennis, R. B. (1994) *Annu. Rev. Biochem. 63*, 675−716.
7. Sone, N., Tsuchiya, N., Inoue, M., and Noguchi, S. (1996) *J. Biol. Chem. 271*, 12457−12462.
8. Yu, J., and Le Brun, N. E. (1998) *J. Biol. Chem. 273*, 8860−8866.
9. Kramer, D. M., Schoepp, B., Liebl, U., and Nitschke, W. (1997) *Biochemistry 36*, 4203−4211.
10. Wollman, F. A., and Lemaire, C. (1988) *Biochim. Biophys. Acta 933*, 85−94.
11. Allen, J. F., Bennett, J., Steinback, K. E., and Arntzen, C. J. (1981) *Nature 291*, 25−29.
12. Zito, F., Finazzi, G., Delosme, R., Nitschke, W., Picot, D., and Wollman, F. A. (1999) *EMBO J. 18*, 2961−2969.
13. Finazzi, G., Zito, F., Barbagallo, R. P., and Wollman, F. A. (2001) *J. Biol. Chem. 276*, 9770−9774.
14. Kallas, T. (1994) in *The Molecular Biology of Cyanobacteria* (Bryant, D. A., Ed.) pp 259−317, Kluwer Academic Publishers, Dordrecht, The Netherlands.
15. Martinez, S. E., Huang, D., Szczepaniak, A., Cramer, W. A., and Smith, J. L. (1994) *Structure 2*, 95−105.
16. Huang, D., Everly, R. M., Cheng, R. H., Heymann, J. B., Schagger, H., Sled, V., Ohnishi, T., Baker, T. S., and Cramer, W. A. (1994) *Biochemistry 33*, 4401−4409.
17. Pierre, Y., Breyton, C., Lemoine, Y., Robert, B., Vernotte, C., and Popot, J. L. (1997) *J. Biol. Chem. 272*, 21901−21908.

18. Hamel, P., Olive, J., Pierre, Y., Wollman, F.-A., and de Vitry, C. (2000) *J. Biol. Chem. 275*, 17072−17079.
19. Chain, R. K., and Malkin, R. (1979) *Arch. Biochem. Biophys. 197*, 52−56.
20. Mitchell, P. (1975) *FEBS Lett. 59*, 137−139.
21. Crofts, A. R., and Wang, Z. (1989) *Photosynth. Res. 22*, 69−87.
22. Trumpower, B. L. (1990) *J. Biol. Chem. 265*, 11409−11412.
23. Crofts, A. R. (1985) in *The Enzymes of Biological Membranes* (Martonosi, A. N., Ed.) pp 347−382, Plenum Publishing, New York.
24. Brandt, U., and Trumpower, B. (1994) *Crit. Rev. Biochem. Mol. Biol. 29*, 165−197.
25. Brandt, U. (1996) *Biochim. Biophys. Acta 1275*, 41−46.
26. Snyder, C. H., Gutierrez-Cirlos, E. B., and Trumpower, B. L. (2000) *J. Biol. Chem. 275*, 13535−13541.
27. Kramer, D. M., and Crofts, A. R. (1993) *Biochim. Biophys. Acta 1183*, 72−84.
28. Sacksteder, C. A., Kanazawa, A., Jacoby, M. E., and Kramer, D. M. (2000) *Proc. Natl. Acad. Sci. U.S.A. 97*, 14283−14288.
29. Brandt, U. (1998) *Biochim. Biophys. Acta 1365*, 261−268.
30. Brandt, U., and von Jagow, G. (1991) *Eur. J. Biochem. 195*, 163−170.
31. Brandt, U. (1996) *FEBS Lett. 387*, 1−6.
32. Crofts, A. R., Guergova-Kuras, M., Huang, L., Kuras, R., Zhang, Z., and Berry, E. A. (1999) *Biochemistry 38*, 15791−15806.
33. Zhang, Z., Huang, L., Shulmeister, V. M., Chi, Y. I., Kim, K. K., Hung, L. W., Crofts, A. R., Berry, E. A., and Kim, S. H. (1998) *Nature 392*, 677−684.
34. Iwata, S., Lee, J. W., Okada, K., Lee, J. K., Iwata, M., Rasmussen, B., Link, T. A., Ramaswamy, S., and Jap, B. K. (1998) *Science 281*, 64−71.
35. Hunte, C., Koepke, J., Lange, C., Rossmanith, T., and Michel, H. (2000) *Struct. Fold. Des. 8*, 669−684.
36. Izrailev, S., Crofts, A. R., Berry, E. A., and Schulten, K. (1999) *Biophys. J. 77*, 1753−1768.
37. Riedel, A., Rutherford, A. W., Hauska, G., Muller, A., and Nitschke, W. (1991) *J. Biol. Chem. 266*, 17838−17844.
38. Brugna, M., Rodgers, S., Schricker, A., Montoya, G., Kazmeier, M., Nitschke, W., and Sinning, I. (2000) *Proc. Natl. Acad. Sci. U.S.A. 97*, 2069−2074.
39. Schoepp, B., Brugna, M., Riedel, A., Nitschke, W., and Kramer, D. M. (1999) *FEBS Lett. 450*, 245−250.
40. Prince, R. C., Crowder, M. S., and Bearden, A. J. (1980) *Biochim. Biophys. Acta 592*, 323−337.
41. Link, T. A., and von Jagow, G. (1995) *J. Biol. Chem. 270*, 25001−25006.
42. Skulachev, V. P., Chistyakov, V. V., Jasaitis, A. A., and Smirnova, E. G. (1967) *Biochem. Biophys. Res. Commun. 26*, 1−6.
43. Nicholls, P., and Malviya, A. N. (1968) *Biochemistry 7*, 305−310.
44. Lorusso, M., Cocco, T., Sardanelli, A. M., Minuto, M., Bonomi, F., and Papa, S. (1991) *Eur. J. Biochem. 197*, 555−561.
45. Kleiner, D. (1974) *Arch. Biochem. Biophys. 165*, 121−125.
46. Rao, B. K. S., Tyryshkin, A. M., Roberts, A. G., Bowman, M. K., and Kramer, D. M. (1999) *Biochemistry 38*, 3285−3296.
47. Berry, E. A., Zhang, Z., Bellamy, H. D., and Huang, L. (2000) *Biochim. Biophys. Acta 1459*, 440−448.
48. Carrell, C. J., Zhang, H., Cramer, W. A., and Smith, J. L. (1997) *Structure 5*, 1613−1625.
49. Iwata, S., Saynovits, M., Link, T. A., and Michel, H. (1996) *Structure 4*, 567−579.
50. Arnon, D. I. (1949) *Plant Physiol. 24*, 1−15.
51. Renganathan, M., and Bose, S. (1990) *Photosynth. Res. 23*, 95−99.
52. Hurt, E., and Hauska, G. (1981) *Eur. J. Biochem. 117*, 591−599.
53. Hauska, G. (1986) *Methods Enzymol. 126*, 271−285.
54. Deutscher, M. P., Simon, M. I., and Abelson, J. N. (1997) *Guide to Protein Purification*, Academic Press, San Diego, CA.
55. Rutherford, A. W., and Setif, P. (1990) *Biochim. Biophys. Acta 1019*, 128−132.
56. Blasie, J. K., Erecinska, M., Samuels, S., and Leigh, J. S. (1978) *Biochim. Biophys. Acta 501*, 33−52.
57. More, C., Belle, V., Asso, M., Fournel, A., Roger, G., and Guigliarelli, B. (1999) *Biospectroscopy 5*, S3−S18.
58. Guigliarelli, B., Guillaussier, J., More, C., Setif, P., Bottin, H., and Bertrand, P. (1993) *J. Biol. Chem. 268*, 900−908.
59. Poole, C. P., Jr. (1983) *Electron Spin Resonance: A Comprehensive Treatise on Experimental Techniques*, 2nd ed., Dover Publications, Inc., Mineola, NY.
60. Pilbrow, J. R. (1990) *Transition Ion Electron Paramagnetic Resonance*, 1st ed., Clarendon Press, Oxford, U.K.
61. Vanngard, T. (1972) in *Biological Applications of Electron Spin Resonance* (Swartz, H. M., Bolton, J. R., and Borg, D. C., Eds.) pp 411−447, Wiley-Interscience, New York.
62. Peisach, J., and Blumberg, W. E. (1974) *Arch. Biochem. Biophys. 165*, 691−708.
63. Solomon, E. I., Penfield, K. W., and Wilcox, D. E. (1983) *Struct. Bond. 53*, 1−57.
64. Solomon, E. I., Baldwin, M. J., and Lowery, M. D. (1992) *Chem. Rev. 92*, 521−542.
65. Weaver, E. C. (1968) *Biochim. Biophys. Acta 162*, 286−289.
66. Utschig, L. M., Poluektov, O., Schlesselman, S. L., Thurnauer, M. C., and Tiede, D. M. (2001) *Biochemistry 40*, 6132−6141.
67. Aronoff-Spencer, E., Burns, C. S., Avdievich, N. I., Gerfen, G. J., Peisach, J., Antholine, W. E., Ball, H. L., Cohen, F. E., Prusiner, S. B., and Millhauser, G. L. (2000) *Biochemistry 39*, 13760−13771.
68. Grogan, J., McKnight, C. J., Troxler, R. F., and Oppenheim, F. G. (2001) *FEBS Lett. 491*, 76−80.
69. Bertocci, U., and Wagman, D. D. (1985) in *Standard Potentials in Aqueous Solution* (Bard, A. J., Parsons, R., and Jordan, J., Eds.) pp 287−293, Marcel Dekker, Inc., New York.
70. Huie, R. E., and Neta, P. (1999) in *Reactive Oxygen Species in Biological Systems: An Interdisciplinary Approach* (Gilbert, D. L., and Colton, C. A., Eds.) pp 33−73, Kluwer Academic/Plenum Publishers, New York.
71. Chevion, M., Berenshtein, E., and Zhu, B.-Z. (1999) in *Reactive oxygen species in biological systems* (Gilbert, D. L., and Colton, C. A., Eds.) pp 103−131, Kluwer Academic/Plenum Publishers, New York.
72. Brodd, R. J., and Werth, J. (1985) in *Standard Potentials in Aqueous Solution* (Bard, A. J., and Parsons, R., Eds.) pp 249−257, Marcel Dekker, Inc., New York.
73. Trumpower, B. L. (1981) *Biochim. Biophys. Acta 639*, 129−155.
74. Link, T. A., and Iwata, S. (1996) *Biochim. Biophys. Acta 1275*, 54−60.
75. Malkin, R. (1981) *Isr. J. Chem. 21*, 301−305.
76. Roberts, A. G., and Kramer, D. M. (2001) *Biochemistry 40*, 13407−13412.
77. Prince, R. C., Linkletter, S. J. G., and Dutton, P. L. (1981) *Biochim. Biophys. Acta 635*, 132−148.
78. Malkin, R. (1982) *Biochemistry 21*, 2945−2950.
79. Baes, C. F., and Mesmer., R. E. (1976) *The Hydrolysis of Cations*, Wiley, New York.
80. Rao B. K., S. (1998) Mechanism and Location of Inhibitory Copper in b_6f Complex: Modes of Copper Inhibition Different in Photosystem I, b_6f complex and Photosystem II, Ph.D. Thesis, Washington State University, Pullman, WA.
81. Crowder, M. S., Prince, R. C., and Bearden, A. (1982) *FEBS Lett. 144*, 204−208.
82. Taylor, C. P. (1977) *Biochim. Biophys. Acta 491*, 137−48.
83. Bergström, J., and Vanngard, T. (1982) *Biochim. Biophys. Acta 682*, 452−456.
84. Widger, W. R., Cramer, W. A., Herrmann, R. G., and Trebst, A. (1984) *Proc. Natl. Acad. Sci. U.S.A. 81*, 674−678.

85. von Jagow, G., and Link, T. A. (1986) *Methods Enzymol. 126*, 253−271.
86. Link, T. A., Haase, U., Brandt, U., and Jagow, G. v. (1993) *J. Bioenerg. Biomembr. 25*, 221−232.
87. Ohnishi, T., and Trumpower, B. L. (1980) *J. Biol. Chem. 255*, 3278−3284.
88. Meinhardt, S. W., and Ohnishi, T. (1992) *Biochim. Biophys. Acta 1100*, 67−74.
89. Barbagallo, R. P., Finazzi, G., and Forti, G. (1999) *Biochemistry 38*, 12814−12821.
90. von Jagow, G., and Ohnishi, T. (1985) *FEBS Lett. 185*, 311−315.
91. Brandt, U., Schagger, H., and von Jagow, G. (1988) *Eur. J. Biochem. 173*, 499−506.
92. Baymann, F., Robertson, D. E., Dutton, P. L., and Mantele, W. (1999) *Biochemistry 38*, 13188−13199.
93. Gurbiel, R. J., Batie, C. J., Sivaraja, M., True, A. E., Fee, J. A., Hoffman, B. M., and Ballou, D. P. (1989) *Biochemistry 28*, 4861−4871.
94. Gurbiel, R. J., Doan, P. E., Gassner, G. T., Macke, T. J., Case, D. A., Ohnishi, T., Fee, J. A., Ballou, D. P., and Hoffman, B. M. (1996) *Biochemistry 35*, 7834−7845.
95. Bertrand, P., Guigliarelli, B., Gayda, J.-P., Beardwood, P., and Gibson, J. F. (1985) *Biochim. Biophys. Acta 831*, 261−266.
96. Schoepp, B., Breton, J., Parot, P., and Vermeglio, A. (2000) *J. Biol. Chem. 275*, 5284−5290.
97. Mosser, G., Breyton, C., Olofsson, A., Popot, J. L., and Rigaud, J. L. (1997) *J. Biol. Chem. 272*, 20263−20268.
98. Iwata, M., Bjorkman, J., and Iwata, S. (1999) *J. Bioenerg. Biomembr. 31*, 169−175.

BI015996K